European Journal of Medicinal Chemistry 203 (2020) 112605

Contents lists available at ScienceDirect

European Journal of Medicinal Chemistry

journal homepage: http://www.elsevier.com/locate/ejmech

Research paper

Novel NHC-coordinated ruthenium(II) arene complexes achieve synergistic efficacy as safe and effective anticancer therapeutics

Chao Chen [a, b], Chang Xu [a], Tongyu Li [a], Siming Lu [c], Fangzhou Luo [a], Hangxiang Wang [a, *]

[a] The First Affiliated Hospital, Key Laboratory of Combined Multi-Organ Transplantation, Ministry of Public Health, School of Medicine, Zhejiang University, Hangzhou, 310003, PR China
[b] College of Life Sciences, Huzhou University, Huzhou, 313000, PR China
[c] Department of Laboratory Medicine, The First Affiliated Hospital, School of Medicine, Zhejiang University, Hangzhou, 310003, PR China

ARTICLE INFO

Article history:
Received 31 March 2020
Received in revised form
16 June 2020
Accepted 18 June 2020
Available online 12 July 2020

Keywords:
N-heterocyclic carbene
Ruthenium(II) complex
Metallodrugs
Anticancer activity
Anti-Metastasis

ABSTRACT

There is an urgent need for more effective, less toxic cancer therapy agents. Motivated by this need, we synthesized a small panel of *N*-heterocyclic carbene (NHC)-coordinated ruthenium(II) arene complexes **Ru1**–**Ru6** with the formula [Ru(*p*-cymene)(L)Cl]PF_6 (L = NHC ligand with varying substituents). Cell-based *in vitro* studies revealed that despite the structural similarity, **Ru1**–**Ru6** exhibited distinct cytotoxic activities against cancer cells. In particular, **Ru4** and **Ru6**, which bear n-octyl and pentamethylbenzyl motifs, respectively, were the most active at inducing apoptosis. In human ovarian A2780 cancer cells, **Ru4** and **Ru6** showed the highest cytotoxicities with IC_{50} values of 2.74 ± 0.15 μM and 1.98 ± 0.10 μM, respectively, and they were approximately 2-fold more potent than cisplatin (IC_{50} = 5.55 ± 0.37 μM). In addition to the cell killing capacity, inhibition of cell migration was validated by using these two optimized complexes. Mechanistic studies revealed that **Ru4** and **Ru6** complexes induced apoptosis in a caspase-dependent manner, primarily through intracellular reactive oxygen species (ROS) overproduction and cell cycle arrest at G1 phase. Furthermore, in a preclinical metastatic model of A2780 tumor xenograft, administration of **Ru4** and **Ru6** (20 μmol/kg) resulted in a marked inhibition of tumor progression and metastasis. Finally, a substantially alleviated systemic toxicity was observed for both complexes in comparison with cisplatin in animals. Overall, this study greatly increases our understanding of NHC-coordinated Ru(II) arene metallodrugs, aiding further investigation of their therapeutic potential in the treatment of metastatic cancers.

1. Introduction

Cancer remains one of the deadliest diseases worldwide, and it constantly evolves to resist and adapt to therapeutic insults [1]. Since the discovery of cisplatin [2], platinum-based chemotherapeutic agents have been widely used as standard-of-care drugs for the treatment of many types of cancer in the clinic [3]. However, dose-limiting side effects (e.g., nephrotoxicity and hepatotoxicity) and intrinsic or acquired drug resistance greatly limit the efficacy of platinum drugs [4]. These intrinsic drawbacks stress the need to develop more effective and less toxic anticancer therapies. In line with this need, a variety of nonplatinum metal complexes have been designed and investigated, some of which have entered clinical trials [5]. Among various types of metallodrugs, ruthenium compounds have attracted significant interest as alternative anticancer drug candidates [6]. Ruthenium possesses similar physiochemical properties to the iron family in the periodic table, which confers the ability to bind various biological macromolecules with less impact on normal cells. More importantly, ruthenium complexes also have low systemic toxicity [7,8], high antitumor activity, and anti-metastatic or anti-angiogenic properties [9–11]. For example, low-toxic ruthenium complexes [imiH]*trans*-[Ru(*N*-imi)(*S*-dmso)Cl_4] (NAMI-A) [12] and [Na]*trans*-[Ru(*N*-ind)$_2Cl_4$] (NKP1339) [13] effectively inhibit tumor metastasis and angiogenesis, and both of them have entered clinical trials. Unfortunately, metallodrugs that can be used as successfully as platinum drugs are still lacking [14].

In the continuing search for effective anticancer ruthenium-based agents, half-sandwich ruthenium(II) (Ru(II)) arene complexes

* Corresponding author. The First Affiliated Hospital, School of Medicine, Zhejiang University, 79, Qingchun Road, Hangzhou, 310003, China.
E-mail address: wanghx@zju.edu.cn (H. Wang).

https://doi.org/10.1016/j.ejmech.2020.112605
0223-5234/

coordinated with various coligands have attracted a surge of attention [15]. In these complexes, the arene ligands are relatively inert towards substitutions, which stabilizes the low oxidation state of Ru(II) complexes under physiological conditions. Consequently, Ru(II) arene complexes can be adjusted to have high hydrophobicity and are also kinetically similar to platinum(II) complexes [16]. Serving as coligands, mono- or bidentate ligands containing different donor atoms have been incorporated to achieve high stability and concurrently, enhance pharmacologic potency [17–20]. Meanwhile, the size and hydrophobicity of arene substituents and the bulky structures of coligands also affect the biological activity of Ru(II) arene complexes [21–25]. Therefore, the structural variability makes these half-sandwich scaffold complexes ideal for construction of pharmacologically active agents. Additionally, unlike platinum-based drugs that exert cytotoxicity primarily through DNA damage, Ru(II) arene complexes usually show multiple mechanisms on cancer cells [26–29] and may potentially address cisplatin resistance by combining synergistic effects [30].

In the ongoing exploration of Ru(II) arene complexes, we constructed novel Ru(II) arene complexes that were coordinated with *N*-heterocyclic carbene (NHC) ligands and explored their efficacy as metallodrugs against cancer cells. NHC is a class of ligands with strong coordination ability, which makes them sufficiently stable under harsh physiological conditions [31]. The structure of NHC ligands can vary widely for metallodrug optimization. Hartinger and Liu et al. have described some pyridyl-NHC [32] and imine-NHC [33] coordination Ru(II) arene complexes in which the introduction of different substituents on the NHC ligands produced metal complexes with extremely different anticancer activities. These results suggest that substituent variation of the NHC ligands can be used to generate effective Ru(II) arene complexes. In particular, by exploiting the NHC ligands with biologically active heterocyclic groups, the anticancer synergy of designed metallodrugs could be anticipated by targeting different intracellular biomolecules.

In this study, a small panel of benzothiazole-functionalized NHC–Ru(II) arene complexes (i.e., **Ru1**–**Ru6**) with altering substituents were synthesized. The substituents with the planar benzothiazole group may facilitate the intercalation of metallodrugs with DNA through π-π stacking, which potentially increases the drug activity. *In vitro* cytotoxicity studies showed that **Ru4** with n-octyl and **Ru6** with pentamethylbenzyl displayed the most potent cytotoxicity. Compared with clinically used cisplatin at the same doses, **Ru4** and **Ru6** were less toxic in animals. In a preclinical metastatic model of human ovarian A2780 xenograft, administration of **Ru4** and **Ru6** resulted in a marked inhibition of tumor progression and metastasis. These data provide compelling evidence that these novel NHC–Ru(II) arene complexes have great therapeutic potential for the treatment of cancers with metastases.

2. Results and discussion

2.1. Synthesis and characterization of N-heterocyclic carbene (NHC)-functionalized Ru(II) arene complexes

Incorporating functional substituents into the NHC moiety is an effective way to construct intriguingly organometallic complexes, and this approach effectively modulates the biological activity of metallodrugs [34]. Inspired by this rationale, we herein designed and synthesized a small library of NHC-functionalized Ru(II) arene complexes bearing a rigid, planar benzothiazole motif (Scheme 1). The NHC precursors (HL(PF_6), L1-L6) were constructed by reacting 2-chlorobenzothiazole with various *N*-substituted imidazole derivatives. Subsequently, the reaction of the imidazole salts HL(PF_6) (L1-L6) with Ag_2O followed by reaction with [Ru(*p*-cymene)Cl_2]$_2$ in

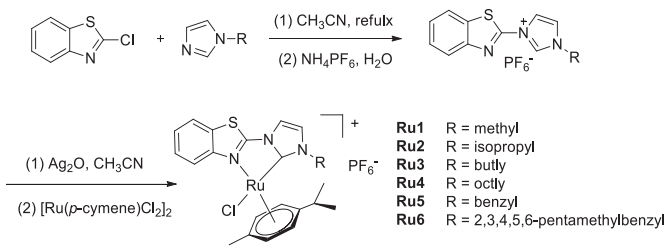

Scheme 1. Synthetic scheme for benzothiazole functionalized *N*-heterocyclic carbene (NHC) ligands and the corresponding Ru–NHC complexes (**Ru1**–**Ru6**).

acetonitrile conveniently yielded NHC–Ru(II) arene complexes (**Ru1**–**Ru6**). The structures of NHC–Ru(II) arene complexes were fully characterized by NMR spectra (e.g., ^{1}H and ^{13}C NMR) and elemental analysis. In the NMR spectra, disappearance of the imidazolium C2–H protons at approximately 10.0 ppm and concurrent appearance of the *p*-cymene protons confirmed the formation of *p*-cymene-coordinated NHC–Ru(II) complexes. Furthermore, the typical downfield carbon signal of Ru-carbene at approximately 188 ppm also verified the formation of the desired final metal complexes.

Additionally, as a representative of these Ru–NHC complexes, the structure of **Ru2** was further confirmed by X-ray single-crystal diffraction analysis. A single crystal of **Ru2** was obtained by slow diffusion of ether into its acetonitrile solution. As expected, **Ru2** adopts a typical three-legged piano stool structure (Fig. 1). The center Ru ion is hex-coordinated with one η^6-coordinated *p*-cymene group, one carbon atom of imidazolylidene ligand, one nitrogen atom of benzothiazole, and one chloride. Similar to other thiazole-functionalized NHC compounds, the sulfur atom on the thiazole ring is away from the coordinated center. The bond angles between the three piano legs N–Ru–C (76.09°), C–Ru–Cl (84.27°) and N–Ru–Cl (87.37°) in **Ru2** are all within the normal range of similar ruthenium-NHC complexes with a *p*-cymene group. Due to the strong coordination ability of imidazolylidene, the bond length of Ru–C (2.030 Å) is shorter than that of Ru–N (2.131 Å) and Ru–Cl (2.384 Å). It is worth noting that the rings of the imidazolylidene and the benzothiazole in **Ru2** are approximately coplanar with the small dihedral angle of 11.05°.

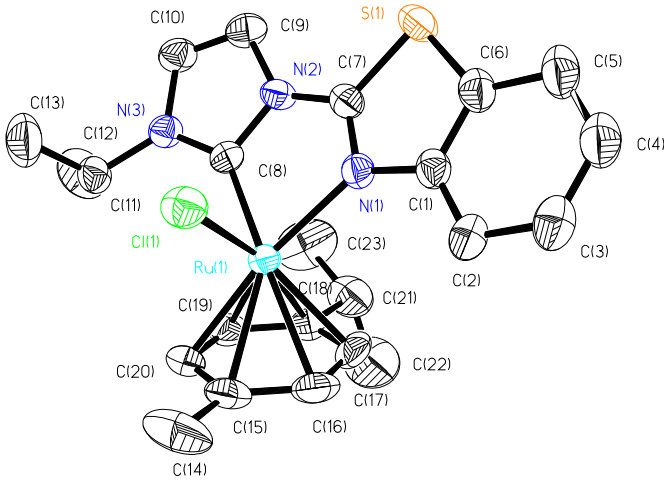

Fig. 1. ORTEP drawing of **Ru2** showing atomic numbering scheme at 50% probability ellipsoids. Selected bond lengths (Å) and angles(deg): Ru(1)–C(8) 2.030(4), Ru(1)–N(1) 2.131(3), Ru(1)–Cl(1) 2.384(12), Ru(1)–C(19) 2.174(4), Ru(1)–C(17) 2.182(4), Ru(1)–C(20) 2.191(4), Ru(1)–C(18) 2.212(4), Ru(1)–C(16) 2.271(4), Ru(1)–C(15) 2.285(4), C(8)-Ru(1)-N(1) 76.09(14), C(8)-Ru(1)-Cl(1) 84.27(11), N(1)-Ru(1)-Cl(1) 87.37(9).

2.2. Examination of in vitro cytotoxicity

Having these compounds in hand, we first evaluated their *in vitro* cytotoxic potentials against six distinct human cancer cell lines, including nonsmall cell lung cancer A549 and HT-29, colon cancer HCT-116 and LoVo, cervical cancer HeLa, and ovarian cancer A2780 cells. The clinically used cisplatin was included as a control. As shown in Table 1 and Fig. S1, although these Ru−NHC complexes are structurally similar, their cytotoxicity varies greatly. **Ru1**−**Ru3** complexes with short alkyl substituents (methyl, isopropyl, and butyl, respectively) showed negligible activities with IC_{50} values larger than 100 μM in all tested cancer cells. However, the **Ru4** complex bearing n-octyl substituent was effective against cancer cells, especially in HT-29 and A2780 cells with IC_{50} values of 8.51 ± 0.69 and 2.74 ± 0.15 μM, respectively. Obviously, the length of the alkyl substituents had a significant effect on the cytotoxicity of these Ru−NHC complexes. Additionally, the potency of **Ru5** and **Ru6** complexes was modulated by the peripheral substituent groups. **Ru5** with a benzyl group was less active in A549 cells and showed moderate activity in HCT-116, LoVo, and HeLa cells. In sharp contrast, **Ru6** bearing a pentamethylbenzyl group exhibited distinguishingly high cytotoxicity against all cancer cells, even greater than that of cisplatin in A2780 cells (e.g., IC_{50} value was approximately 2.5-fold lower than cisplatin). Collectively, the order of *in vitro* cytotoxicity for these complexes is **Ru6** > **Ru4** > **Ru5** > **Ru1**, **Ru2**, **Ru3**. These results provided an implication that small modifications the substituent of metal complexes greatly affect their biological activity.

A previous study indicated that lipophilicity of metallodrugs plays a vital role in their antitumor activities [35]. Therefore, we determined the oil-water distribution coefficients (log $P_{o/w}$) of these complexes using the "shaking flask" method. As shown in Table 1, the log $P_{o/w}$ values of for these complexes ranged from 0.51 to 0.92. Of note, the **Ru4** and **Ru6** complexes showed high lipophilicity, which makes both compounds more likely to penetrate the cell membrane. To further elucidate the substituent-activity relationship, cellular uptake of complexes was measured with **Ru1**, **Ru2**, **Ru4**, and **Ru6** as model complexes. After 3 or 6 h of incubation, the metal concentrations in A2780 cells were analyzed by inductively coupled plasma mass (ICP-MS) spectrometry. As shown in Fig. S2, compared with the **Ru1** and **Ru2** treatment, exposure of cells to the **Ru4** and **Ru6** complexes resulted in significantly higher accumulation in A2780 cells. Collectively, these results provide evidence that the superior cytotoxicity of **Ru4** and **Ru6** is associated with substituents of longer alkyl and polysubstituted aryl moieties, which eventually increase the lipophilicity of the entire NHC−Ru(II) arene complex, cellular uptake and thereby, cytotoxic potency.

Upon system administration, the complexes will encounter serum proteins and noncovalent interactions occur, which may reduce the drug activity. Therefore, we monitored the UV−vis spectral changes of the **Ru4** and **Ru6** complexes when incubated in fetal bovine serum (FBS) with 10% (v/v) dimethyl sulfoxide (DMSO). As a result, the spectra of both complexes showed negligible changes after incubation for two days, indicating that they are potentially stable during systemic circulation (Fig. S3). Additionally, we incubated the two complexes with mouse serum at 37 °C for two days and further tested the cytotoxic activity in A2780 cells by the MTT assay. The results suggested that pre-incubation with mouse serum did not compromise their activity (IC_{50} = 3.24 ± 0.17 μM for **Ru4** and 2.64 ± 0.13 μM for **Ru6**) (Fig. S4). Thus, these data showed that the **Ru4** and **Ru6** complexes maintain stability under complicated biological conditions.

2.3. Anti-proliferation activity

Having identified that **Ru4** and **Ru6** are promising chemotherapeutic agents, we further investigated their anti-proliferation activity in A2780 cells using the EdU (5-ethynyl-2′-deoxyuridine) incorporation assay. EdU is an alkyne-tagged thymine nucleoside derivative that can be incorporated into replicating DNA during cell proliferation. Subsequently, the EdU moiety can be labeled with a green fluorescent dye by a click reaction and used to detect DNA replication activity. Compared with the untreated cells in which the average proliferation ratio was 53%, cisplatin (2 μM) slightly decreased the proliferation ratio to 49% (Fig. 2). After treatment with **Ru4** or **Ru6** (2 μM) for 24 h, the average proliferation ratio of A2780 cells significantly decreased to 38% and 37%, respectively. Furthermore, when the drug concentrations increased to 4 μM, the proliferation ratios dramatically decreased to 15% and 16% for **Ru4**- and **Ru6**-treated cells, respectively, which were significantly lower than those for 4 μM cisplatin-treated cells (34%). These results showed that these Ru(II) arene metallodrugs effectively impede cancer cell proliferation in a dose-dependent manner.

2.4. Anti-migration assay

In addition to the anti-proliferation activity, the ability to inhibit cancer cell migration is important for chemotherapeutic drugs in the treatment of metastatic cancer. Previous studies have shown that ruthenium complexes with aromatic groups such as Ru(II)-acylthiourea [36] and Ru(II)-pcymene-amino oxime [37] exhibit high inhibitory effects on the migration of cancer cells. Therefore, we next explored the anti-migration capability of these Ru(II) arene complexes in A2780 cancer cells using a wound-healing assay. For this purpose, monolayer cells plated in 12-well plates were scratched and washed with PBS. Then, the complexes at different concentrations in FBS-free medium were added to suppress cell migration. As shown in Fig. 3, the wound healing of A2780 cancer cells was markedly reduced after 24 h treatment with Ru(II) complexes (4 μM) compared to untreated cells and cisplatin-treated cells. For example, the mean wound closure ratio of A2780 was 33.3% in untreated cells, whereas treatment with **Ru4** or **Ru6** dramatically reduced the migration ratios to 11.7% and 8.7%,

Table 1
IC_{50} values (μM) of **Ru1**−**Ru6** complexes and cisplatin (*cis*-**Pt**) against a small panel of human cancer cell lines after 48 h of drug exposure. The cell viability was determined by the MTT assay. The data are presented as the means ± SD (n = 4). The log $P_{o/w}$ values were determined *via* the "shaking flask" method against n-octanol/water (1:1, v/v) partition.

Cell line	Ru1	Ru2	Ru3	Ru4	Ru5	Ru6	*cis*-Pt
A549	>100	>100	>100	24.6 ± 2.36	>100	19.6 ± 1.47	16.6 ± 0.75
HT-29	>100	>100	>100	5.20 ± 0.31	8.51 ± 0.69	3.17 ± 0.22	8.19 ± 0.35
HCT-116	>100	>100	>100	25.6 ± 1.67	43.5 ± 2.54	12.8 ± 0.68	6.74 ± 0.45
LoVo	>100	>100	>100	19.4 ± 0.58	56.8 ± 4.78	11.9 ± 0.31	8.58 ± 0.36
Hela	>100	>100	>100	39.1 ± 1.35	55.5 ± 1.04	23.0 ± 0.46	10.3 ± 1.13
A2780	>100	84.1 ± 5.24	>100	2.74 ± 0.15	6.61 ± 0.37	1.98 ± 0.10	5.55 ± 0.37
log $P_{O/W}$	0.52	0.51	0.54	0.83	0.77	0.92	–

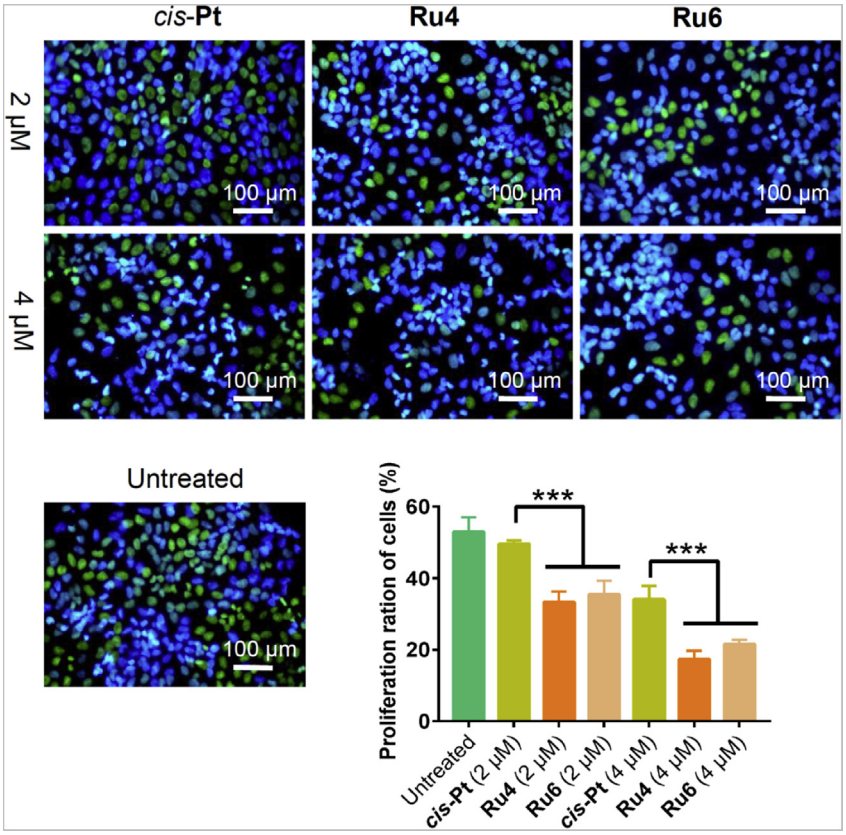

Fig. 2. Anti-proliferation activity of ruthenium complexes **Ru4** and **Ru6** and cisplatin (*cis*-**Pt**). A2780 cells were treated with drugs for 24 h and then analyzed by EdU incorporation assay. Proliferating cells were shown in green and bright blue, and quiescent, nondividing cells were shown in blue. The data are presented as the means ± SD; n > 5 regions with a total of 1500–2000 cells analyzed, ***$p < 0.001$. (For interpretation of the references to colour in this figure legend, the reader is referred to the Web version of this article.)

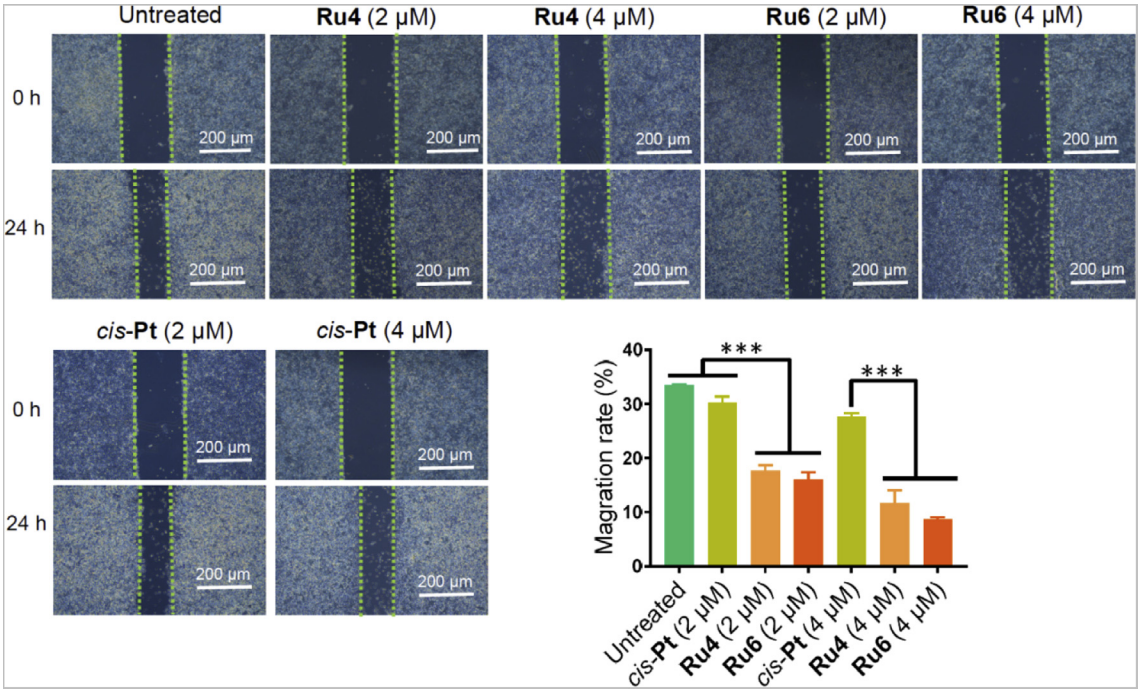

Fig. 3. Wound-healing assay performed on A2780 cells. Cells were treated with **Ru4**, **Ru6**, or cisplatin at concentrations of 2 or 4 μM for 24 h. The data are presented as the means ± SD (n = 3), ***$p < 0.001$.

respectively. In contrast, cisplatin showed negligible activity at preventing cell migration. Additionally, a dose-dependent activity to inhibit migration of cancer cells was observed using both the **Ru4** and **Ru6** complex, which is consistent with results observed in antiproliferative assays.

2.5. NHC–Ru(II) arene complexes induce apoptosis in cancer cells

The results of cell-based *in vitro* experiments clearly evidenced that **Ru4** and **Ru6** had superior antitumor activities among others in cancer cells. To further explore anticancer activity, we investigated how these complexes evoked cell death. Morphological change of cells is a preliminary indicator of cells responding to cytotoxic agents. After exposing A2780 cells to **Ru4**, **Ru6**, or cisplatin for 24 h, the cells were stained with AO/EB dyes and observed under fluorescence microscopy. AO penetrates all cells and emits green fluorescence, whereas EB only passes through broken cell membranes and interacts with DNA, emitting orange fluorescence [38]. As shown in Fig. 4, healthy A2780 cells showed a fusiform structure with green fluorescence. Treatment with 4 μM cisplatin produced a negligible effect observed in AO/EB staining. This may be attributable to A2780 cells overcoming the cisplatin effect at low concentrations over a short duration by cell protection mechanisms. However, after 24 h of treatment with **Ru4** or **Ru6** at 4 μM, the cell morphology was rounded and cells displayed typical condensed orange chromatin. This image indicated that the cell protection mechanisms of A2780 had been disturbed under the action of **Ru4** or **Ru6**, and EB had entered the cells. Furthermore, cell rounding is usually a sign of apoptosis. Thus, the AO/EB assay suggests that NHC–Ru(II) arene complexes (e.g., **Ru4** and **Ru6**) present here disrupt cell membrane integrity and evoke cell death.

To further clarify the mode-of-action of these complexes, the Annexin V-FITC/PI apoptosis assay was conducted in A2780 cells and analyzed by flow cytometry. Annexin V-FITC is a fluorescently labeled phospholipid-binding protein, which can bind to phosphatidylserine in early apoptotic cells. PI cannot penetrate normal cells and early apoptotic cells, but it can penetrate late apoptotic and necrotic cells and stain the nucleus. Thus, the combined use of two dyes can distinguish cells at different stages. After treatment with cisplatin and **Ru4** and **Ru6** complexes (4 μM) for 48 h, the total populations of early apoptotic cells increased to 37.4%, 78.2%, and 84.3%, respectively (Fig. 5a and 5b). In sharp contrast, there were few late apoptotic and necrotic cells (PI-positive) observed, with the populations less than 8.5% (Fig. 5a). We further performed Western blot analysis to verify the mechanism of **Ru4** and **Ru6** in inducing cell death. Treatment of **Ru4** and **Ru6** increased the expression of several key apoptosis-associated proteins [39] such as cleaved PARP (c-PARP), cleaved caspase-3 and caspase-9, which was consistent with observations in cells treated with cisplatin (Fig. 5c). Thus, our results clearly demonstrated that **Ru4** and **Ru6** exert their anticancer activity primarily *via* the apoptotic pathway.

2.6. Mechanistic studies of NHC–Ru(II) arene complexes against cancer cells

Next, the mode of action using the **Ru4** and **Ru6** complexes against cancer cells was investigated. Previous studies have demonstrated that the main cytotoxic activity of metal complexes against cancer cells is caused by overproduction of intracellular reactive oxygen species (ROS) [40]. Therefore, we first measured ROS production in A2780 cells using a ROS indicator, 6-carboxy-2′,7′-dichlorodihydrofluorescein diacetate (DCFH-DA). Upon uptake by cells, DCFH-DA can be hydrolyzed and oxidized to produce green fluorescence in the presence of ROS. Thus, the fluorescence emission correlates with the level of ROS in cells. As shown in Fig. 6a, after treatment with **Ru4** or **Ru6** at 4 μM for 12 h, A2780 cells displayed a higher green fluorescence signal than untreated cells and cisplatin-treated cells. The flow cytometry analysis also showed that cells treated with the metal complexes overproduced ROS, resulting in increased fluorescence intensity (Fig. 6b). As is well known, mitochondria are the main organelle for ROS production. During mitochondrial respiration, a small number of electrons leak out of the mitochondrial electron transport chain and encounter O_2 to generate ROS. Therefore, overproduction of ROS indicates that mitochondrial respiration has been disrupted. To confirm the role of mitochondria in ROS production, we used a well-established mitochondria indicator, JC-1 (5,5′,6,6′-tetrachloro-1,1′,3,3′-tetraethylbenzimidazolyl carbocyanine iodide), to study the changes of mitochondrial membrane potential in A2780 cells. As shown in Fig. 6c, the JC-1 dye labeled the mitochondrial matrix

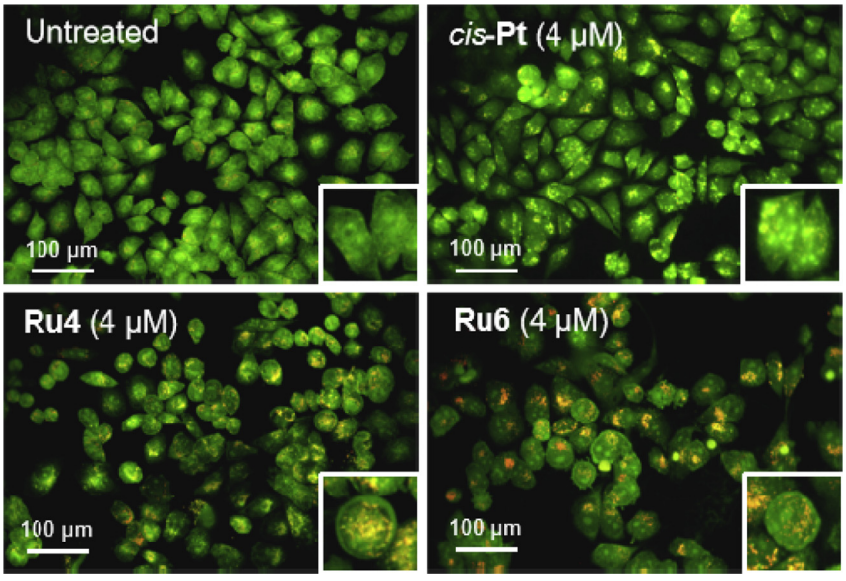

Fig. 4. Representative images of AO/EB dual staining of untreated, **Ru4**, **Ru6**, and cisplatin (4 μM) A2780 cells after 24 h of treatment.

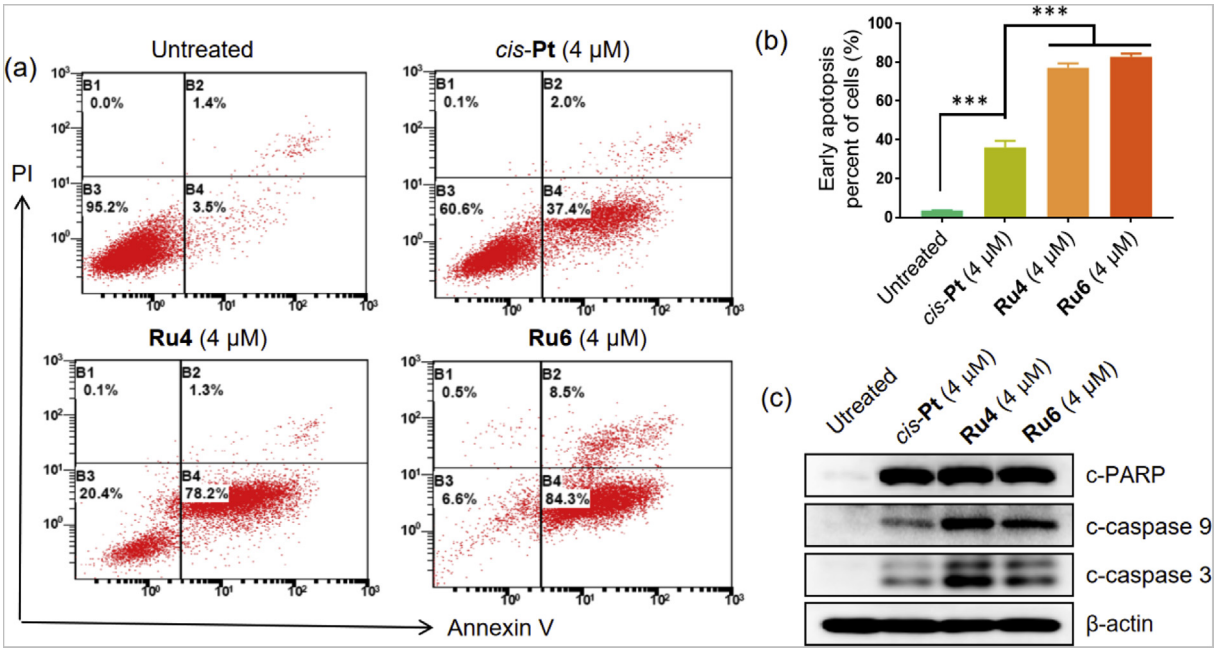

Fig. 5. (a, b) Apoptosis in response to treatment with **Ru4**, **Ru6**, and cisplatin (4 μM, 48 h) was determined by Annexin V/PI double-staining assay. (c) Western blot analysis to examine the expression of apoptosis-associated proteins in A2780 cells after treatment with **Ru4**, **Ru6**, and cisplatin (4 μM) for 24 h.

of untreated normal cells and formed orange-emitting aggregates. When the mitochondrial membrane potential is destroyed, JC-1 dye will not be able to accumulate in the mitochondria and emit green fluorescence. As expected, after 24 h of treatment with **Ru4** or **Ru6**, A2780 cells emitted green fluorescence with reduced orange fluorescence, suggesting mitochondrial dysfunction induced by the NHC—Ru(II) arene complexes. This result was further supported by flow cytometry analysis (Fig. 6d). Treatment of A2780 cells with Ru complexes significantly increased the green fluorescence ratio of JC-1 from 7.64% (untreated cells) to 44.41% (**Ru4**-treated cells) and 50.63% (**Ru6**-treated cells), respectively. However, the effect of cisplatin is very minor, as green fluorescence signal only increased to 18.48% after 24 h treatment with the same drug concentration.

Considering these results, we speculate on the potential mode of action causing cell death. Negatively charged mitochondria could be the major target of **Ru4** and **Ru6** in cells. Upon uptake by cancer cells, the cationic moiety of the complexes could interact with mitochondria, and then depolarize the mitochondrial membrane potential. This could further disrupt cell respiration and produce excess ROS. Eventually, oxidative stress could cause significant damage to various intracellular (bio)molecules, thereby affecting their normal biochemical functions and leading to apoptosis.

As shown in previous studies [39,41], cell cycle arrest is another major cause of apoptosis. We therefore examined the effect of **Ru4** and **Ru6** on cycle distribution of A2780 cells, and cisplatin was used as a control. After 24 h of treatment with **Ru4**, **Ru6**, and cisplatin at 4 μM, cells were harvested and analyzed by flow cytometry (Fig. 7). As expected, the untreated cells showed a normal cycle distribution, with the mean population percentages of G1 (50.88%), S (28.68%) and G2/M (20.43%). The cisplatin-treated cells showed a slightly decreased population in G1 (43.71%), increased population in S (36.66%), and approximately equal population in G2/M (19.62%). This could be explained by cisplatin exerting its anticancer activity mainly through DNA interactions (blocking in S phase). **Ru4** and **Ru6** showed G1 phase arrest activity. After exposure to **Ru4** or **Ru6** for 24 h, A2780 cells displayed a significant increase in G1 phase, with mean population percentages of 70.16% and 74.74%, respectively (Fig. 7). G1 phase is the presynthesis phase of DNA. When cells are arrested in this phase, progression from G1 to S and G2/M phase slows down and eventually leads to cell swelling and apoptosis. Moreover, G1 phase arrest of these Ru(II) complexes indicates that interaction with DNA is not the main anticancer mechanism of **Ru4** and **Ru6**, although they had multiple modes of action in the cells. Hence, the distinct mechanism endowed by these complexes makes them useful anticancer drug candidates for the treatment of cancers with cisplatin resistance.

2.7. *In vivo systemic toxicity*

Intrigued by the *in vitro* potential including potent cytotoxic and anti-migration activity, we aimed to assess the antitumor activity of **Ru4** and **Ru6** in animals. Prior to therapeutic studies, the *in vivo* toxicity of both complexes was investigated in ICR mice. For this purpose, the compounds were dissolved in DMSO/saline (1:1, v/v) solution and intraperitoneally injected into healthy ICR mice ($n = 8$ in each group) at different doses (10 and 20 μmol/kg). Cisplatin was also administered as a reference. Following five injections, the changes in body weight of these mice were recorded to assess the drug toxicity (Fig. 8a). When the body weight loss of the mice exceeds 20%, we consider the administered drugs highly toxic. Previous studies have shown that cisplatin can cause a significant reduction in the body weight of mice [42]. Five injections of cisplatin at a dose of 10 μmol/kg caused six out of eight mice to lose more than 20% of their body weight in 15 days. Encouragingly, **Ru4** and **Ru6** complexes were well tolerated in animals at this dose. For instance, the mice treated with **Ru4** or **Ru6** at doses of 10 μmol/kg did not show body weight loss. We further increased the dose of the drugs to 20 μmol/kg for five intraperitoneal injections. As shown in Fig. 8a, the mice still showed considerable tolerance to the high doses of the Ru(II) complexes. Only two **Ru4**- and one **Ru6**-treated mice lost over 20% of body weight after five successive injections. In sharp contrast, all mice injected with cisplatin at a dose of 20 μmol/kg lost more than 20% of their body weights within 15 days. These results provided compelling evidence that NHC—Ru(II) arene

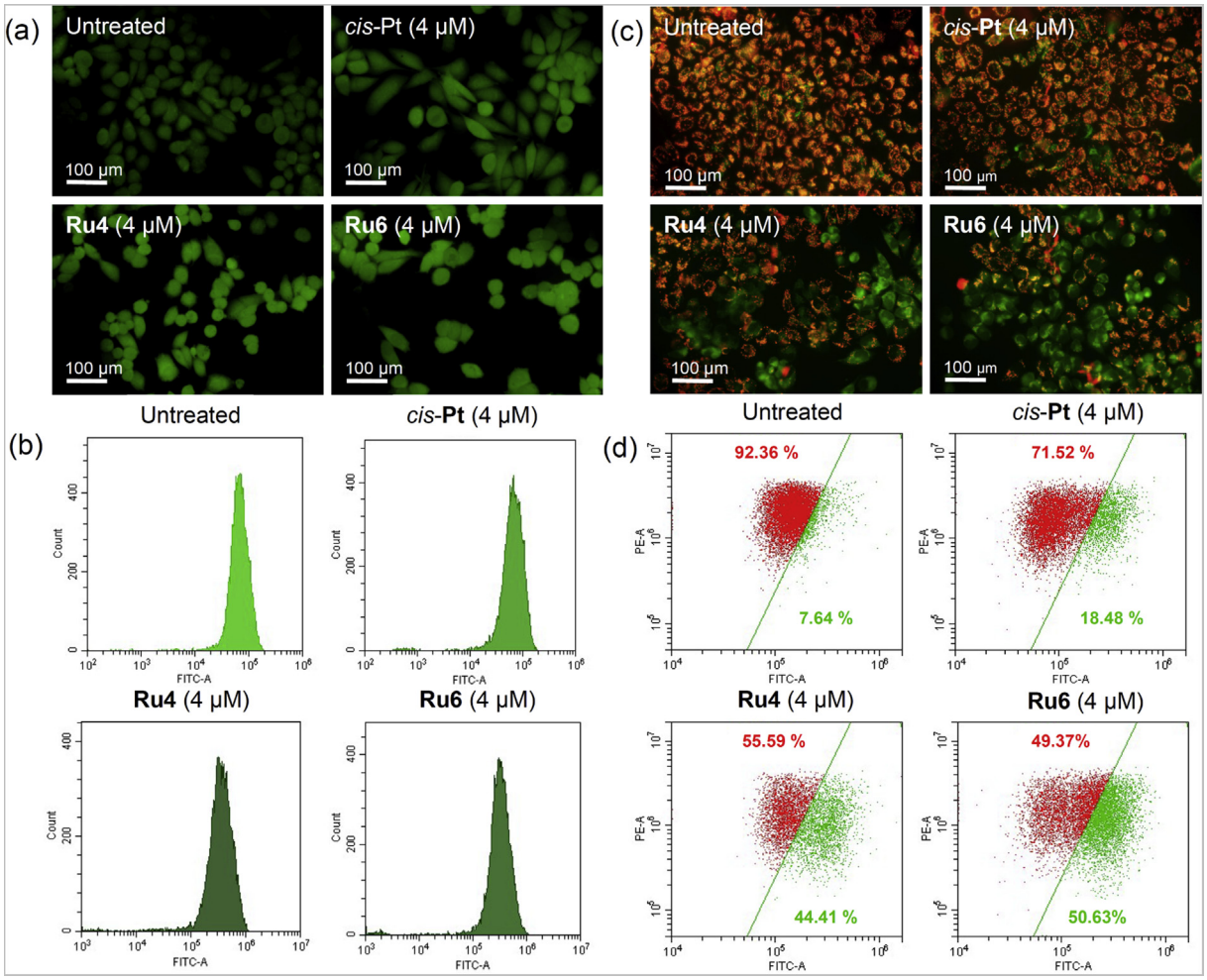

Fig. 6. (a) Representative images of DCFH-DA-stained A2780 cells after treatment with **Ru4**, **Ru6**, and cisplatin (4 μM) for 12 h. (b) Representative histograms displaying ROS production as determined by flow cytometry analysis. The cells were treated with **Ru4**, **Ru6**, and cisplatin (4 μM) for 12 h. (c) Fluorescence microscopy images of JC-1 staining after A2780 cells were treated with **Ru4**, **Ru6**, and cisplatin (4 μM) of 24 h. (d) Changes in the mitochondrial membrane potential in A2780 cells after 24 h.

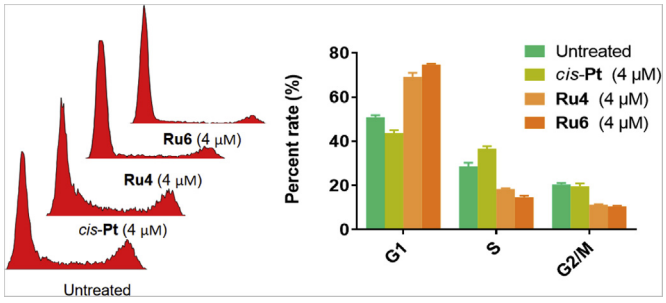

Fig. 7. Flow cytometry analysis of cell cycle distribution. A2870 cancer cells were exposed to **Ru4**, **Ru6**, and cisplatin (4 μM) for 24 h. The data are presented as the means ± SD (n = 3).

complexes possess higher safety margins compared to the clinically used cisplatin agent. Though the mechanisms underlying the low toxicity remain unclear, we reasonably envision that stable coordination of ruthenium metal to NHC ligands contributes to the reduced toxicity of these Ru(II) complexes, which deserves further investigation.

2.8. Therapeutic efficacy in a preclinical metastatic model of human A2780 cancer

Encouraged by reduced drug toxicity in animals, we therefore evaluated the *in vivo* anticancer efficacy of Ru(II) arene complexes in comparison with cisplatin in Balb/c nude mice bearing A2780 cell-derived ovarian cancer. Each mouse in treatment groups (n = 8 in each group) was intraperitoneally injected with 200 μL of A2780 cells suspension (5×10^7 cells/mL in PBS). Starting the next day, we initiated therapy by intraperitoneally administering drugs in 200 μL of DMSO/saline (1:1, v/v) solution. Body weights were recorded during the experiment, and tumors and ovaries were collected for evaluation at the end of the study. To avoid potential toxicity, drug administration was reduced to three times on day 0, 3, and 6. Thus, the body weight of the mice treated with **Ru4** and **Ru6** decreased slightly in the initial days but immediately rebounded after cessation of treatment (Fig. 8b). However, cisplatin-treated mice showed substantial weight loss (above 20%). This result again confirmed that at the same doses, **Ru4** and **Ru6** were less toxic than cisplatin in mice. Administration of **Ru4** and **Ru6** at the dose of 20 μmol/kg yielded mean tumor growth inhibition (TGI) rates of 65.2%, and 68.7%, respectively (Fig. 8a and 8b). Compared with cisplatin treatment with a TGI rate of 36.7%, **Ru4** and **Ru6** treatments showed superior antitumor efficacy. More

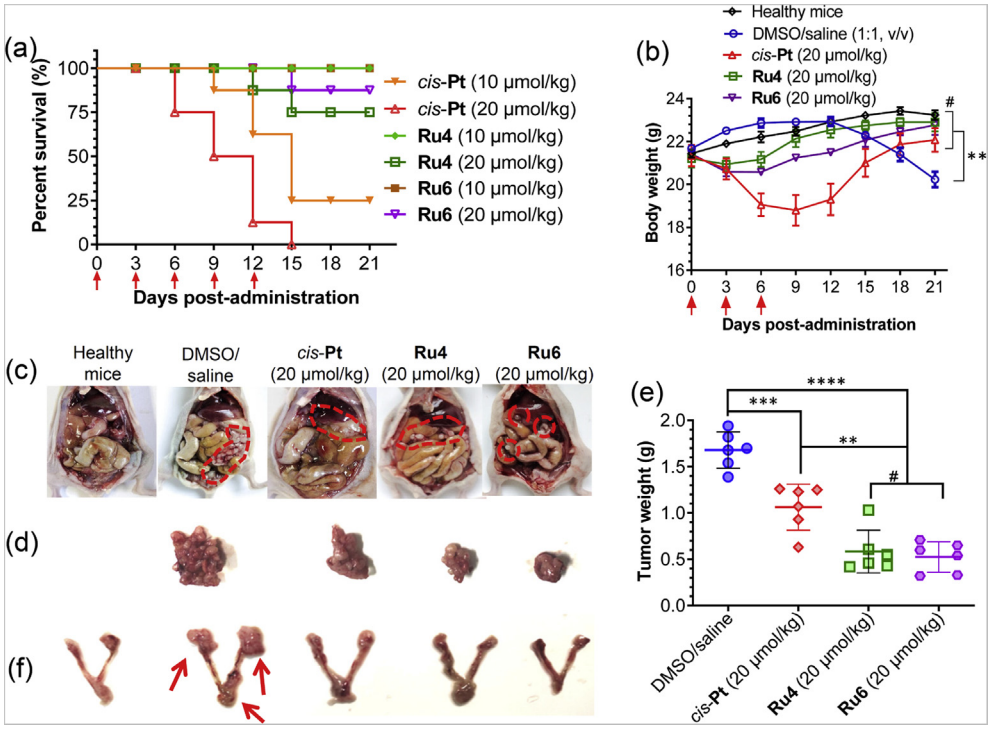

Fig. 8. (a) Survival of healthy ICR mice following intraperitoneal injection of saline, cisplatin, **Ru4**, and **Ru6** for five successive times every other day. The mice were defined as dead when body weight loss exceeded 20%. Arrows indicate intraperitoneal injections. (b) Body weights of nude mice were measured to evaluate drug toxicity. (c) Photographs of tumor-bearing nude mice after treatments. (d) Total tumor weight excised from the mice after different treatments and in each group at the end of the study. (e, f) Representative images of tumors and ovaries. Healthy mice without tumor cell implantation were used as controls, and the data are presented as the means ± SD (n = 8 in each group); $^{**}p < 0.01$, and $^{***}p < 0.001$.

significantly, **Ru4** and **Ru6** suppressed metastasis of cancer cells to ovaries. The ovary in Ru(II) complex-treated mice had normal morphology; however, cancer cells clearly migrated to the ovaries and uterus in DMSO/saline-treated mice (Fig. 8f). Metastasis accounts for the majority of cancer-associated death in patients, and it remains a significant therapeutic challenge. The compounds

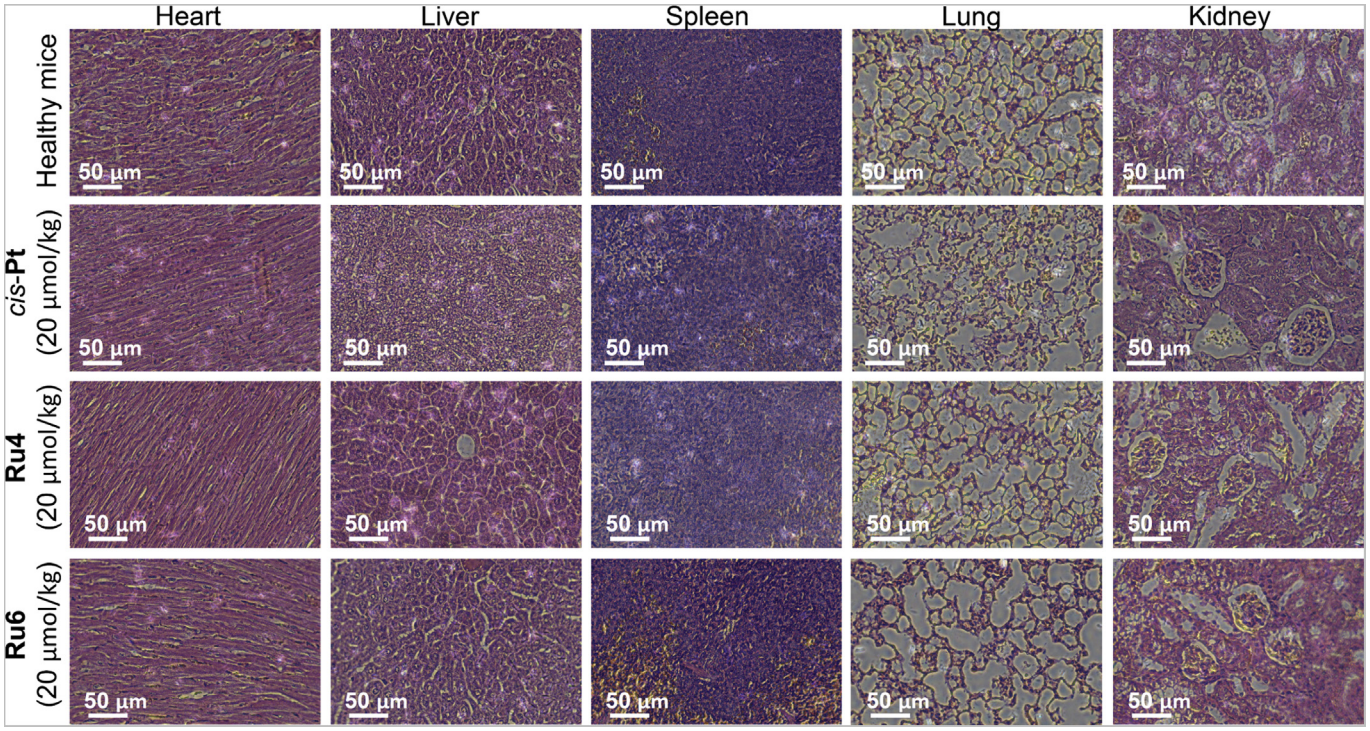

Fig. 9. Representative H&E staining of the major tissues (e.g., heart, liver, spleen, lung, and kidney) excised from the different treatment groups.

presented here not only suppressed the growth of bulky primary tumors but also reduced the metastatic burden to other organs. Therefore, such multifunctional agents could greatly benefit the long-term survival of patients in future clinical use.

Previous studies have suggested that nephrotoxicity and hepatotoxicity are the major side effects for the clinic use of the cisplatin drug [43]. Cases of pulmonary toxicity have also been reported [44]. We hypothesized that **Ru4** and **Ru6** were able to reduce organ toxicity in animals. Following administration of drugs, the main organs (e.g., heart, liver, spleen, lung, and kidney) from each group were excised and subjected to histological analysis (Fig. 9). In cisplatin-treated mice, we found that hepatocytes exhibited extensive inflammatory response, dissolution of cytoplasm, and necrosis. The livers of **Ru4**- and **Ru6**-treated mice presented the similar pathological characteristics with that of saline-treated mice. In kidneys, cisplatin treatment resulted in the collapse of glomeruli. Encouragingly, no nephrotoxicity was observed in **Ru4**- and **Ru6**-treated mice. In cisplatin-treated mice, the lung displayed local inflammation with the diffused damage of pulmonary alveoli. **Ru4**- and **Ru6**-treated mice showed similar pathology but less severe. Additionally, the morphology of other tissues (e.g., heart and spleen) in drug-treated mice are similar to that of the saline-treated mice. Together, these *in vivo* studies revealed that **Ru4** and **Ru6** can effectively inhibit tumor growth and metastasis and have good tolerability in mice, as evidenced by this metastatic A2780 tumor model.

3. Conclusion

In summary, we synthesized and characterized a series of promising Ru(II) arene complexes (**Ru1**−**Ru6**) bearing benzothiazole-functionalized NHC ligands. The *in vitro* cell-based studies demonstrated that **Ru4** and **Ru6** complexes are potent anticancer agents across distinct cancer cell types. Given the intrinsic feature of NHC−Ru(II) arene complexes in circumventing cisplatin resistance and their synergistic modes of action and low toxicity [31,33,45,46], these new NHC−Ru(II) arene complexes may be of potential use in cancer patients with impaired renal function and deserve further investigation.

4. Experimental section

4.1. Materials and methods for synthesis of Ru(II) arene complexes

2-Chlorobenzothiazole and $[(\eta^6\text{-}p\text{-cym})RuCl_2]_2$ were purchased from TCI (Shanghai, China). All other chemicals were of reagent-grade quality, obtained from commercial sources and used as received. Chromatographic purification was accomplished using flash column chromatography on silica gel (neutral, Qingdao Haiyang Chemical Co., Ltd). ^{1}H and ^{13}C NMR spectra were recorded on a Bruker Avance-400 (400 MHz) spectrometer at 400 MHz for ^{1}H and 100 MHz for ^{13}C. Chemical shifts (δ) are expressed in ppm downfield to TMS at = 0 ppm and coupling constants (J) are expressed in Hz. Elemental analyses were performed with a Flash EA 1112 from ThermoFinnigan. Crystal data collection and reduction were performed using the Oxford Diffraction CrysAlisPro software. The structure of **Ru2** was solved by direct methods, and the nonhydrogen atoms were subjected to anisotropic refinement by full-matrix least squares on *F*2 using the SHELXTXL package. Crystal data of **Ru2** are in Table S1, and CCDC 1992990 contains the supplementary crystallographic data for this paper.

4.1.1. General procedure for synthesis of benzothiazole-functionalized imidazolium salts HLPF6 (L1-L6)

Imidazole derivatives (6 mmol) and 2-chlorobenzothiazole (5 mmol) were mixed in 20 mL acetonitrile and heated overnight. The resulting solid was separated and dissolved in water, and then a saturated $NH4PF_6$ aqueous solution was added. The resulting precipitate was obtained as white solid. Yield: 65−83%. NMR data and spectrum are shown in support information.

4.1.2. Synthesis of benzothiazole functionalized NHC− Ru(II)-arene complexes (Ru1−Ru6)

A mixture of respective imidazolium salt $HLPF_6$ (0.5 mmol) and silver oxide (0.3 mmol) in 10 mL CH_3CN was stirred at 50 °C for 12 h. After cooling to room temperature, $[Ru(p\text{-cymene})Cl_2]_2$ (0.25 mmol) was added to the mixture and stirred for another 6 h. The resulting orange solution was filtered through Celite, concentrated under reduced pressure and purified by flash column chromatography.

[(*p*-cymene)Ru(L1)Cl](PF6) (**Ru1**).

Orange solid, Yield: 236 mg (75%). ^{1}H NMR (400 MHz, DMSO-d_6) δ (ppm): 8.58, 7.91 (both d, J = 2.0 Hz, imidazole CH, 2H), 8.38, 8.31 (both d, J = 8.0 Hz, benzothiazole CH, 2H), 7.85, 7.70 (t, J = 8.0 Hz, benzothiazole CH, 2H), 6.81, 6.63, 6.35, 5.87 (both d, J = 6.0 Hz, *p*-cym-H, 4H), 4.20 (s, CH3, 3H), 2.30-2.23 (m, *p*-cym C*H*$(CH_3)_2$, 1H), 2.16 (s, *p*-cym CH_3, 3H), 0.81, 0.76 (both d, J = 6.4 Hz, *p*-cym CH(C*H*$_3)_2$, 6H). ^{13}C NMR (100 MHz, DMSO-d_6): δ (ppm) 188.3 (Ru−C), 161.7, 147.4, 130.7, 129.3, 127.9, 127.3, 125.2, 121.8, 118.7, 89.7, 87.7, 38.6, 30.9, 22.5, 19.2. Anal. Calc. for $C_{21}H_{23}ClF_6N_3PRuS$: C, 39.97; H, 3.67; N, 6.66. Found: C, 39.86; H, 3.47; N, 6.83.

[(*p*-cymene)Ru(L2)Cl](PF6) (**Ru2**).

Orange solid, Yield: 247 mg (78%). ^{1}H NMR (400 MHz, DMSO-d_6) δ (ppm): 8.66, 8.18 (both d, J = 2.4 Hz, imidazole CH, 2H), 8.38, 8.31 (both d, J = 8.0 Hz, benzothiazole CH, 2H), 7.86, 7.70 (t, J = 8.0 Hz, benzothiazole CH, 2H), 6.77, 6.42, 6.32, 5.87 (both d, J = 6.0 Hz, *p*-cym-H, 4H), 5.05-4.98 (m, s, C*H*$(CH_3)_2$, 1H), 2.28-2.24 (m, *p*-cym C*H*$(CH_3)_2$, 1H), 2.26 (s, *p*-cym CH_3, 3H), 1.79, 1.45 (both d, J = 6.8 Hz, *p*-cym CH(C*H*$_3)_2$, 6H), 0.83, 0.79 (both d, J = 6.8 Hz, *p*-cym CH(C*H*$_3)_2$, 6H). ^{13}C NMR (100 MHz, DMSO-d_6): δ (ppm) 186.7 (Ru−C), 161.7, 147.5, 130.7, 129.3, 127.2, 125.2, 123.1, 121.8, 119.9, 89.6, 87.6, 54.4, 24.0, 22.8, 22.6, 22.4, 19.2. Anal. Calc. for $C_{23}H_{27}ClF_6N_3PRuS$: C, 41.92; H, 4.13; N, 6.38. Found: C, 42.06; H, 4.10; N, 6.35.

[(*p*-cymene)Ru(L3)Cl](PF6) (**Ru3**).

Orange solid, Yield: 212 mg (63%). ^{1}H NMR (400 MHz, DMSO-d_6) δ (ppm): 8.61, 8.00 (both d, J = 2.4 Hz, imidazole CH, 2H), 8.38, 8.31 (both d, J = 8.0 Hz, benzothiazole CH, 2H), 7.84, 7.70 (t, J = 8.0 Hz, benzothiazole CH, 2H), 6.76, 6.56, 6.36, 5.80 (both d, J = 6.0 Hz, *p*-cym-H, 4H), 4.58-4.45 (m, CH2, 2H), 2.28-2.22 (m, *p*-cym C*H*$(CH_3)_2$, 1H), 2.14 (s, *p*-cym CH_3, 3H), 1.97-1.90 (m, CH2, 2H), 1.45-1.30 (m, CH2, 2H), 0.95 (t, J = 7.2 Hz, CH3, 3H), 0.81, 0.78 (both d, J = 7.2 Hz, *p*-cym CH(C*H*$_3)_2$, 6H). ^{13}C NMR (100 MHz, DMSO-d_6): δ (ppm) 187.3 (Ru−C), 161.6, 147.5, 130.7, 129.3, 127.2, 126.6, 125.1, 121.8, 118.9, 89.7, 87.5, 51.4, 32.2, 30.9, 22.4, 19.7, 19.2, 14.1. Anal. Calc. for $C_{24}H_{29}ClF_6N_3PRuS$: C, 42.83; H, 4.34; N, 6.24. Found: C, 42.77; H, 4.25; N, 6.19.

[(*p*-cymene)Ru(L4)Cl](PF6) (**Ru4**)

Orange solid, Yield: 219 mg (60%). ^{1}H NMR (400 MHz, DMSO-d_6) δ (ppm): 8.60, 8.00 (both d, J = 2.4 Hz, imidazole CH, 2H), 8.49, 8.33 (both d, J = 8.0 Hz, benzothiazole CH, 2H), 7.84, 7.70 (t, J = 8.0 Hz, benzothiazole CH, 2H), 6.76, 6.56, 6.36, 5.79 (both d, J = 5.6 Hz, *p*-cym-H, 4H), 4.55−4.45 (m, CH2, 2H), 2.26−2.23 (m, *p*-cym C*H*$(CH_3)_2$, 1H), 2.14 (s, *p*-cym CH_3, 3H), 1.96−1.92 (m, CH2, 2H), 1.38−1.26 (m, CH_2, 10H), 0.86 (t, J = 7.2 Hz, CH_3, 3H), 0.81, 0.78 (both d, J = 6.8 Hz, *p*-cym CH(C*H*$_3)_2$, 6H). ^{13}C NMR (100 MHz, DMSO-d_6): δ (ppm) 187.3 (Ru−C), 161.6, 147.5, 130.7, 129.3, 127.2, 126.6, 125.2, 121.9, 119.0, 89.7, 87.5, 51.6, 31.7, 30.9, 30.2, 29.1, 29.0, 26.4, 22.6, 22.5, 19.2, 14.4. Anal. Calc. for $C_{28}H_{37}ClF_6N_3PRuS$: C, 46.12; H, 5.11; N, 5.76. Found: C, 45.98; H, 5.14; N, 5.82.

[(*p*-cymene)Ru(L5)Cl](PF6) (**Ru5**)

Orange solid, Yield: 251 mg (71%).^{1}H NMR (400 MHz, DMSO-d_6)

δ (ppm): 8.63, 7.74 (both d, $J = 2.4$ Hz, imidazole CH, 2H), 8.39, 8.33 (both d, $J = 8.0$ Hz, benzothiazole CH, 2H), 7.86, 7.71 (t, $J = 8.0$ Hz, benzothiazole CH, 2H), 7.51–7.40 (m, C_6H_5, 5H), 6.78 (d, $J = 6.0$ Hz, *p*-cym-H, 1H), 6.36, (t, $J = 6.0$ Hz, *p*-cym-H, 2H), 5.93 (d, $J = 6.0$ Hz, *p*-cym-H, 1H), 5.76 (q, $J = 15.2$ Hz CH2, 2H), 2.28–2.21 (m, *p*-cym C*H*$(CH_3)_2$, 1H), 2.16 (s, *p*-cym CH_3, 3H), 0.80, 0.75 (both d, $J = 6.8$ Hz, *p*-cym CH(C*H*$_3)_2$, 6H). ^{13}C NMR (100 MHz, DMSO-d_6): δ (ppm) 188.4 (Ru–C), 161.8, 147.4, 136.0, 130.8, 129.4, 129.3, 129.0, 128.9, 127.3, 126.4, 125.2, 121.8, 119.7, 89.7, 87.8, 55.0, 30.8, 22.4, 19.2, 15.6. Anal. Calc. for $C_{27}H_{27}ClF_6N_3PRuS$: C, 45.86; H, 3.85; N, 5.94. Found: C, 45.89; H, 3.74; N, 6.03.

[(*p*-cymene)Ru(L6)Cl](PF6) (**Ru6**)

Orange solid, Yield: 245 mg (63%).^{1}H NMR (400 MHz, DMSO-d_6): δ (ppm) 8.49, 6.95 (both d, $J = 2.4$ Hz, imidazole CH, 2H), 8.37, 8.35 (both d, $J = 8.0$ Hz, benzothiazole CH, 2H), 7.86, 7.70 (t, $J = 8.0$ Hz, benzothiazole CH, 2H), 6.83, 6.79 (both d, $J = 6.0$ Hz, *p*-cym-H, 2H), 6.54, 6.52, (both s, *p*-cym-H, 2H), 5.96, 5.67 (both d, $J = 14.4$ Hz, CH_2, 2H), 2.33–2.14 (m, *p*-cym C*H*$(CH_3)_2$ (1H) + *p*-cym CH_3 (3H) + CH_3 (15H)), 0.88, 0.84 (both s, *p*-cym CH(C*H*$_3)_2$, 6H). ^{13}C NMR (100 MHz, DMSO-d_6): δ (ppm) 187.6 (Ru–C), 161.6, 147.5, 136.3, 134.5, 133.3, 130.8, 129.3, 127.8, 127.3, 126.4, 125.2, 121.9, 119.0, 90.0, 87.3, 50.9, 31.0, 22.5, 19.2, 17.5, 17.1, 15.6. Anal. Calc. for $C_{32}H_{37}ClF_6N_3PRuS$: C, 49.45; H, 4.80; N, 5.41. Found: C, 50.06; H, 4.53; N, 5.55.

4.2. Cell lines and animals

Cells were cultured in medium containing 10% fetal bovine serum (FBS), penicillin (100 units/mL), and streptomycin (100 μg/mL). Cells were maintained in a humid atmosphere at 37 °C with 5% CO_2. Five- to six-week-old ICR and female Balb/c mice were purchased from Shanghai Experimental Animal Center, Chinese Academy of Sciences. All experiments were performed under the guidance of the Zhejiang University Committee for Animal Use and Care. Animal experiments were approved by Zhejiang University Committee, and Zhejiang Experimental Animal Center provided aseptic conditions, autoclaved rodent diet and sterile water. For details of the cell and animals experiments, see supporting information.

4.3. Statistical analysis

All of the quantitative data are presented as the means ± SD. The statistical significance between the measurements was assessed using Student's *t*-test. A p-value less than 0.05 was considered statistically significant, whereas a p-value less than 0.01 was considered highly significant.

Declaration of competing interest

The authors declare no potential conflicts of interest.

Acknowledgement

This work was supported by the National Natural Science Foundation of China (Nos. 81571799 and 81773193), the Zhejiang Province Preeminence Youth Fund (LR19H160002), and the Huzhou University Research Project (Grant No. 2018XJKJ39).

Appendix A. Supplementary data

Supplementary data to this article can be found online at https://doi.org/10.1016/j.ejmech.2020.112605.

References

[1] F. Bray, J. Ferlay, I. Soerjomataram, R.L. Siegel, L.A. Torre, A. Jemal, Global cancer statistics 2018: globocan estimates of incidence and mortality worldwide for 36 cancers in 185 countries, CA, Cancer J Clin 68 (2018) 394–424.
[2] B. Rosenberg, L. Vancamp, T. Krigas, Inhibition of cell division in escherichia coli by electrolysis products from a platinum electrode, Nature 205 (1965) 698–699.
[3] T. Boulikas, M. Vougiouka, Recent clinical trials using cisplatin, carboplatin and their combination chemotherapy drugs (Review), Oncol. Rep. 11 (2004) 559–595.
[4] R. Oun, Y.E. Moussa, N.J. Wheate, The side effects of platinum-based chemotherapy drugs: a review for chemists, Dalton Trans. 47 (2018) 6645–6653.
[5] K.D. Mjos, C. Orvig, Metallodrugs in medicinal inorganic chemistry, Chem. Rev. 114 (2014) 4540–4563.
[6] S. Thota, D.A. Rodrigues, D.C. Crans, E.J. Barreiro, Ru(II) compounds: next-generation anticancer metallotherapeutics, J. Med. Chem. 61 (2018) 5805–5821.
[7] O.A. Lenis-Rojas, M.P. Robalo, A.I. Tomaz, A. Carvalho, A.R. Fernandes, F. Marques, M. Folgueira, J. Yáñez, D. Vázquez-García, M.L. Torres, A. Fernández, J.J. Fernández, RuII(p-cymene) compounds as effective and selective anticancer candidates with no toxicity in vivo, Inorg. Chem. 57 (2018) 13150–13166.
[8] M.K. Mohamed Subarkhan, L. Ren, B. Xie, C. Chen, Y. Wang, H. Wang, Novel tetranuclear ruthenium(ii) arene complexes showing potent cytotoxic and antimetastatic activity as well as low toxicity *in vivo*, Eur. J. Med. Chem. 179 (2019) 246–256.
[9] A. Zamora, S.A. Pérez, V. Rodríguez, C. Janiak, G.S. Yellol, J. Ruiz, Dual antitumor and antiangiogenic activity of organoplatinum(II) complexes, J. Med. Chem. 58 (2015) 1320–1336.
[10] P. Nowak-Sliwinska, C.M. Clavel, E. Păunescu, M.T. te Winkel, A.W. Griffioen, P.J. Dyson, Antiangiogenic and anticancer properties of bifunctional ruthenium(II)-p-cymene complexes: influence of pendant perfluorous chains, Molecular Pharm 12 (2015) 3089–3096.
[11] P. Nowak-Sliwinska, J.R. van Beijnum, A. Casini, A.A. Nazarov, G. Wagnières, H. van den Bergh, P.J. Dyson, A.W. Griffioen, Organometallic ruthenium(II) arene compounds with antiangiogenic activity, J. Med. Chem. 54 (2011) 3895–3902.
[12] J.M. Rademaker-Lakhai, D. van den Bongard, D. Pluim, J.H. Beijnen, J.H.M. Schellens, A phase I and pharmacological study with imidazolium-trans-DMSO-imidazole-tetrachlororuthenate, a novel ruthenium anticancer agent, Clin. Canc. Res. 10 (2004) 3717–3727.
[13] C.G. Hartinger, M.A. Jakupec, S. Zorbas-Seifried, M. Groessl, A. Egger, W. Berger, H. Zorbas, P.J. Dyson, B.K. Keppler, KP1019, A new redox-active anticancer agent- preclinical development and results of a clinical phase I study in tumor patients, Chem. Biodivers. 5 (2008) 2140–2155.
[14] T. Lazarevic, A. Rilak, Z.D. Bugarcic, Platinum, palladium, gold and ruthenium complexes as anticancer agents: current clinical uses, cytotoxicity studies and future perspectives, Eur. J. Med. Chem. 142 (2017) 8–31.
[15] A.K. Singh, D.S. Pandey, Q. Xu, P. Braunstein, Recent advances in supramolecular and biological aspects of arene ruthenium(II) complexes, Coord. Chem. Rev. 270 (2014) 31–56.
[16] G. Süss-Fink, Arene ruthenium complexes as anticancer agents, Dalton Trans. 39 (2010) 1673–1688.
[17] R. Pettinari, F. Marchetti, C.D. Nicola, C. Pettinari, A. Galindo, R. Petrelli, L. Cappellacci, M. Cuccioloni, L. Bonfili, A.M. Eleuteri, M.F.C.G. da Silva, A.J.L. Pombeiro, Ligand design for N,O- or N,N-pyrazolone-based hydrazones ruthenium(II)-arene complexes and investigation of their anticancer activity, Inorg. Chem. 57 (2018) 14123–14133.
[18] J. Li, M. Tian, Z. Tian, S. Zhang, C. Yan, C. Shao, Z. Liu, Half-Sandwich iridium(III) and ruthenium(II) complexes containing P^P-chelating ligands: a new class of potent anticancer agents with unusual redox features, Inorg. Chem. 57 (2018) 1705–1716.
[19] M.M. Haghdoost, J. Guard, G. Golbaghi, A. Castonguay, Anticancer Activity and catalytic potential of Ruthenium(II)-Arene Complexes with N,O-donor ligands, Inorg. Chem. 57 (2018) 7558–7567.
[20] K. Jeyalakshmi, J. Haribabu, C. Balachandran, Srividya Swaminathan, N.S.P. Bhuvanesh, R. Karvembu, Coordination behavior of N,N',N"-trisubstituted guanidine ligands in their Ru arene Complexes: synthetic, DNA/protein binding, and cytotoxic studies, Organometallics 38 (2019) 753–770.
[21] C.M. Clavel, E. Paunescu, P. Nowak-Sliwinska, A.W. Griffioen, R. Scopelliti, P.J. Dyson, Modulating the anticancer activity of ruthenium(II)-Arene Complexes, J. Med. Chem. 58 (2015) 3356–3365.
[22] J. Li, Z. Tian, X. Ge, Z. Xu, Y. Feng, Z. Liu, Design, synthesis, and evaluation of fluorine and naphthyridinee based half-sandwich organoiridium/ruthenium complexes with bioimaging and anticancer activity, Eur. J. Med. Chem. 163 (2019) 830–839.
[23] G. Golbaghi, I. Pitard, M. Lucas, M.M. Haghdoost, Y.L. los Santos, N. Doucet, S.A. Patten, J.T. Sanderson, A. Castongua, Synthesis and biological assessment of a ruthenium(II) cyclopentadienyl complex in breast cancer cells and on the development of zebrafish embryos, Eur. J. Med. Chem. 118 (2020) 112030.
[24] S. Seršen, J. Kljun, K. Kryeziu, R. Panchuk, B. Alte, W. Körner, P. Heffeter, W. Berger, I. Turel, Structure-related mode-of-action differences of anticancer organoruthenium complexes with β-Diketonates, J. Med. Chem. 58 (2015) 3984–3996.
[25] M. Lari, M. Martínez-Alonso, N. Busto, B.R. Manzano, A.M. Rodríguez, M.I. Acuña, F. Domínguez, J.L. Albasanz, J.M. Leal, G. Espino, B. García, Strong influence of ancillary ligands containing benzothiazole or benzimidazole rings

on cytotoxicity and photoactivation of Ru(II) arene complexes, Inorg. Chem. 57 (2018) 14322–14336.
[26] L.A. Hager, S. Mokesch, C. Kieler, S.A. Castro, D. Baier, A. Roller, W. Kandioller, B.K. Keppler, W. Berger, L. Salassa, A. Terenzi, Ruthenium-arene complexes bearing naphthyl-substituted 1,3-dioxoindan-2-carboxamides ligands for G-quadruplex DNA recognition, Dalton Trans. 48 (2019) 12040–12049.
[27] C. Tan, S. Lai, S. Wu, S. Hu, L. Zhou, Y. Chen, M. Wang, Y. Zhu, W. Lian, W. Peng, L. Ji, A. Xu, Nuclear permeable ruthenium(II) β-carboline complexes induce autophagy to antagonize mitochondrial-mediated apoptosis, J. Med. Chem. 53 (2010) 7613–7624.
[28] Z. Tian, J. Li, S. Zhang, Z. Xu, Y. Yang, D. Kong, H. Zhang, X. Ge, J. Zhang, Z. Liu, Lysosome-targeted chemotherapeutics: half-sandwich ruthenium(II) complexes that are selectively toxic to cancer cells, Inorg. Chem. 57 (2018) 10498–10502.
[29] J. Zhao, S. Li, X. Wang, G. Xu, S. Gou, Dinuclear organoruthenium complexes exhibiting antiproliferative activity through DNA damage and a reactive-oxygen-species-mediated endoplasmic reticulum stress pathway, Inorg. Chem. 58 (2019) 2208–2217.
[30] I. Romero-Canelón, L. Salassa, P.J. Sadler, The contrasting activity of iodido versus chlorido ruthenium and osmium arene azo- and imino-pyridine anticancer complexes: control of cell selectivity, cross-Resistance, p53 Dependence, and Apoptosis Pathway, J. Med. Chem. 56 (2013) 1291–1300.
[31] W. Liu, R. Gust, Metal N-heterocyclic carbene complexes as potential anti-tumor metallodrugs, Chem. Soc. Rev. 42 (2013) 755–773.
[32] S. Movassaghi, S. Singh, A. Mansur, K.K.H. Tong, M. Hanif, H.U. Holtkamp, T. Sçhnel, S.M.F. Jamieson, C.G. Hartinger, (Pyridin-2-yl)-NHC organo-ruthenium complexes: antiproliferative properties and reactivity toward biomolecules, Organometallics 37 (2018) 1575–1584.
[33] Y. Yang, L. Guo, Z. Tian, X. Liu, Y. Gong, H. Zheng, X. Ge, Z. Liu, Imine-N-heterocyclic carbenes as versatile ligands in ruthenium(II) *p*-cymene anticancer complexes: a structure-activity relationship study, Chem. Asian J. 13 (2018) 2923–2933.
[34] C. Chen, L. Zhou, B. Xie, Y. Wang, L. Ren, X. Chen, B. Cen, Lv He, H. Wang, Novel fast-acting pyrazole/pyridine-functionalized N-heterocyclic carbene silver complexes assembled with nanoparticles show enhanced safety and efficacy as anticancer therapeutics, Dalton Trans. 49 (2020) 2505–2516.
[35] G. Lv, L. Guo, L. Qiu, H. Yang, T. Wang, H. Liu, J. Lin, Lipophilicity-dependent ruthenium N-heterocyclic carbene complexes as potential anticancer agents, Dalton Trans. 44 (2015) 7324–7733.
[36] L. Colina-Vegas, L. Luna-Dulcey, A.M. Plutín, E.E. Castellano, M.R. Cominetti, A.A. Batista, Half sandwich Ru(ii)-acylthiourea complexes: DNA/HSA-binding, anti-migration and cell death in a human breast tumor cell line, Dalton Trans. 46 (2017) 12865–12875.
[37] Y. Benabdelouahab, L. Muñoz-Moreno, M. Frik, I.d.l. Cueva-Alique, M.A.E. Amrani, M. Contel, A.M. Bajo, T. Cuenca, E. Royo, Hydrogen bonding and anticancer properties of water-soluble chiral *p*-cymene RuII compounds with amino-oxime Ligands, Eur. J. Inorg. Chem. 13 (2015) 2295–2307.
[38] P. Sanpui, A. Chattopadhyay, S.S. Ghosh, Induction of apoptosis in cancer cells at low silver nanoparticle concentrations using chitosan nanocarrier, ACS Appl. Mater. Interfaces 3 (2011) 218–228.
[39] H. Lee, N. Saini, A.B. Parris, M. Zhao, X. Yang, Ganetespib induces G2/M cell cycle arrest and apoptosis in gastric cancer cells through targeting of receptor tyrosine kinase signaling, Int. J. Oncol. 51 (2017) 967–974.
[40] X. Wang, X. Wang, S. Jin, N. Muhammad, Z. Guo, Stimuli-responsive therapeutic metallodrugs, Chem. Rev. 119 (2019) 1138–1192.
[41] S. Xu, H. Yao, S. Luo, Y. Zhang, D. Yang, D. Li, G. Wang, M. Hu, Y. Qiu, X. Wu, H. Yao, W. Xie, Z. Chen, J. Xu, A novel potent anticancer compound optimized from a natural oridonin scaffold induces apoptosis and cell cycle arrest through the mitochondrial pathway, J. Med. Chem. 60 (2017) 1449–1468.
[42] Z. Ma, D. Wang, X. Song, Y. Wu, Q. Chen, C. Zhao, J. Li, S. Cheng, J. Xu, Chlorambucil-conjugated platinum(IV) prodrugs to treat triple-negative breast cancer in vitro and in vivo, Eur. J. Med. Chem. 157 (2019) 1292–1299.
[43] Z. Pezeshki, A. Khosravi, M. Nekuei, S. Khoshnood, E. Zandi, M. Eslamian, A. Talebi, S.N.-e.-d. Emami, M. Nematbakhsh, Time course of cisplatin-induced nephrotoxicity and hepatotoxicity, J Nephropathol 6 (2017) 163–167.
[44] X. Lan, J. She, D. Lin, Y. Xu, X. Li, W. Yang, V. Lui, L. Jin, X. Xie, Y. Su, Microneedle-mediated delivery of lipid-coated cisplatin nanoparticles for efficient and safe cancer therapy, ACS Appl. Mater. Interfaces 39 (2018) 33060–33069.
[45] L. Zeng, P. Gupta, Y. Chen, E. Wang, L. Ji, H. Chao, Z. Chen, The development of anticancer ruthenium(II) complexes: from single molecule compounds to nanomaterials, Chem. Soc. Rev. 46 (2017) 5771–5804.
[46] R.G. Kenny, C.J. Marmion, Toward multi-targeted platinum and ruthenium drugs-a new paradigm in cancer drug treatment regimens, Chem. Rev. 119 (2019) 1058–1137.